\



A novel low-loss four-bit bandpass filter using RF MEMS switches

Lulu Han(韩路路), Yu Wang(王宇), Qiannan Wu(吴倩楠), Shiyi Zhang(张世义), Shanshan Wang(王姗姗), and Mengwei Li(李孟委)

Citation: Chin. Phys. B, 2022, 31 (**1**): 018506. DOI: 10.1088/1674-1056/ac1b95
Journal homepage: http://cpb.iphy.ac.cn; http://iopscience.iop.org/cpb

What follows is a list of articles you may be interested in

A novel multifunctional electronic calibration kit integrated by MEMS SPDT switches

Shan-Shan Wang(王姗姗), Qian-Nan Wu(吴倩楠), Yue-Sheng Gao(高跃升), Jian-Gang Yu(余建刚), Qian-Long Cao(曹钎龙), Lu-Lu Han(韩路路), and Meng-Wei Li(李孟委)

Chin. Phys. B, 2021, 30 (**11**): 118501. DOI: 10.1088/1674-1056/abf12b

Reversible waveform conversion between microwave and optical fields in a hybrid opto-electromechanical system

Li-Guo Qin(秦立国), Zhong-Yang Wang(王中阳), Jie-Hui Huang(黄接辉), Li-Jun Tian(田立君), and Shang-Qing Gong(龚尚庆)

Chin. Phys. B, 2021, 30 (**6**): 068502. DOI: 10.1088/1674-1056/abea8f

Opto-electromechanically induced transparency in a hybrid opto-electromechanical system

Hui Liu(刘慧), Li-Guo Qin(秦立国), Li-Jun Tian(田立君), Hong-Yang Ma(马鸿洋)

Chin. Phys. B, 2019, 28 (**10**): 108502. DOI: 10.1088/1674-1056/ab3af2

Efficient molecular model for squeeze-film damping in rarefied air

Cun-Hao Lu(陆存豪), Pu Li(李普), Yu-Ming Fang(方玉明)

Chin. Phys. B, 2019, 28 (**9**): 098501. DOI: 10.1088/1674-1056/ab3443

Electrically controlled optical switch in the hybrid opto-electromechanical system

Li-Guo Qin(秦立国), Zhong-Yang Wang(王中阳), Hong-Yang Ma(马鸿洋), Shu-Mei Wang(王淑梅), Shang-Qing Gong(龚尚庆)

Chin. Phys. B, 2017, 26 (**12**): 128502. DOI: 10.1088/1674-1056/26/12/128502

A novel low-loss four-bit bandpass filter using RF MEMS switches

Lulu Han(韩路路)[1,2,3,4], Yu Wang(王宇)[1,2,3,4], Qiannan Wu(吴倩楠)[2,3,4,5,†], Shiyi Zhang(张世义)[1,2,3,4], Shanshan Wang(王姗姗)[1,2,3,4], and Mengwei Li(李孟委)[1,2,3,4,‡]

[1] *School of Instrument and Electronics, North University of China, Taiyuan* 030051, *China*
[2] *Nantong Institute of Intelligent Opto-Mechatronics, North University of China, Nantong* 226000, *China*
[3] *Center for Microsystem Integration, North University of China, Taiyuan* 030051, *China*
[4] *Academy for Advanced Interdisciplinary Research, North University of China, Taiyuan* 030051, *China*
[5] *School of Science, North University of China, Taiyuan* 030051, *China*

(Received 13 July 2021; revised manuscript received 5 August 2021; accepted manuscript online 7 August 2021)

This paper details the design and simulation of a novel low-loss four-bit reconfigurable bandpass filter that integrates microelectromechanical system (MEMS) switches and comb resonators. A T-shaped reconfigurable resonator is reconfigured in a 'one resonator, multiple MEMS switches' configuration and used to gate the load capacitances of comb resonators so that a multiple-frequency filtering function is realized within the 7–16 GHz frequency range. In addition, the insertion loss of the filter is less than 1.99 dB, the out-of-band rejection is more than 18.30 dB, and the group delay is less than 0.25 ns. On the other hand, the size of this novel filter is only 4.4 mm × 2.5 mm × 0.4 mm. Our results indicate that this MEMS reconfigurable filter, which can switch 16 central frequency bands through eight switches, achieves a low insertion loss compared to those of traditional MEMS filters. In addition, the advantages of small size are obtained while achieving high integration.

Keywords: four-bit, RF microelectromechanical system (MEMS) switch, reconfigurable filter, comb resonator

PACS: 85.85.+j **DOI:** 10.1088/1674-1056/ac1b95

1. Introduction

Bandpass filters are widely used in microwave and millimeter-wave circuits and systems due to their ability to select or suppress signals at specific frequencies.[1–12] In recent years, great attention has been paid to reconfigurable filters based on various circuit structures, owning to their ability to reduce complexity and strengthen expansibility in modern electronic systems.[13–19]

Traditional reconfigurable filters, including semiconductor filters,[14] and MEMS filters,[15–17,19] have been extensively studied over the last two decades. However, these filters have shortcomings, such as large structural size, complex structure, high loss, and low integration. Chuang *et al.*[14] proposed a switchable filter with a selectable range of 0.9–2.35 GHz based on the use of p–i–n diode switches. The maximum insertion loss of the filter was approximately 3 dB, and the overall size was 97 mm × 32 mm. Since each diode was too complicated to be integrated into a uniplanar filter structure, this reconfigurable bandpass filter had limitations, for instance, a large size and large insertion loss. Moreover, based on MEMS switches, Zhang *et al.*[15] demonstrated an open-loop reconfigurable filter composed of "open-loop" resonators and cantilever MEMS switches with reconfigurable frequency bands of 7.81 GHz and 8.35 GHz, respectively. The insertion loss of this reconfigurable filter in the passband was smaller than 3.4 dB, and its size was 25 mm × 17 mm. Compared with the device described in Ref. [14], its size was greatly reduced, but it was still not conductive to integration into an RF module.

To address the abovementioned problems associated with existing MEMS reconfigurable filters, this study proposes a novel low-loss four-bit filter using RF MEMS switches. It can switch 16 operating states through eight switches in the frequency range of 7–16 GHz, and the overall size of this novel proposed filter is only 4.4 mm × 2.5 mm × 0.4 mm. It can effectively reduce insertion loss, reduce the system size, and improve the reliability of the system.

2. Theory and design

2.1. Design of the MEMS switch

The reconfigurable filter has eight MEMS switches that represent 16 operating states according to their positioning in the 'up' and 'down' states. Ohmic contact MEMS switches are employed to tune the filter frequency,[20,21] the equivalent circuit diagram is shown in Fig. 1, in which Z_{cpw} is the equivalent impedance of a coplanar waveguide (CPW), R_s is the resistance when the switch is "closed", and C_s is the coupling capacitance formed by the cantilever beam and the CPW signal line when the switch is "open".

The cantilever beam of the MEMS switch is a straight plate structure that has the characteristics of a simple struc-

†Corresponding author. E-mail: qiannanwoo@nuc.edu.cn
‡Corresponding author. E-mail: lmwnuc@163.com

© 2022 Chinese Physical Society and IOP Publishing Ltd

ture and is easy to process. Additionally, to facilitate the release of the sacrificial layer and reduce the driving voltage of the MEMS switch, several release holes are designed in the cantilever beam. The structure and simulation results of the MEMS switch are shown in Figs. 2(a) and 2(b), respectively.

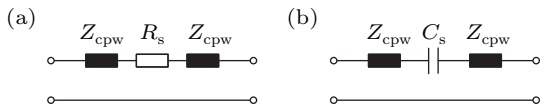


Fig. 1. Equivalent circuit diagram of the ohmic contact MEMS switch: (a) "closed" state and (b) "open" state.

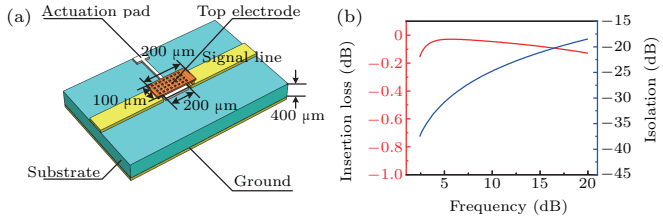


Fig. 2. (a) Structure of the MEMS switch. (b) Simulation results of the MEMS switch.

The elastic coefficient of the straight plate cantilever beam design is mainly determined by the beam stiffness, k. When the driving voltage is applied directly under the cantilever beam, it is equivalent to a distributed load acting on the single-ended cantilever beam. Based on this, the elastic coefficient k of the cantilever beam can be expressed as

$$k = \frac{1}{4} E w \left(\frac{t}{l}\right)^3, \tag{1}$$

where l, w, t, and E are the length, width, thickness, and Young's modulus of the cantilever beam. The elastic coefficient, k_c, of the designed cantilever beam is calculated to be 1.024 N/m. The area between the cantilever beam and the pull-down electrode is $A = 18000$ μm^2, and the distance between the cantilever beam and the pull-down electrode is $g = 3.0$ μm. According to the calculation, the driving voltage is $V = 12.41$ V.

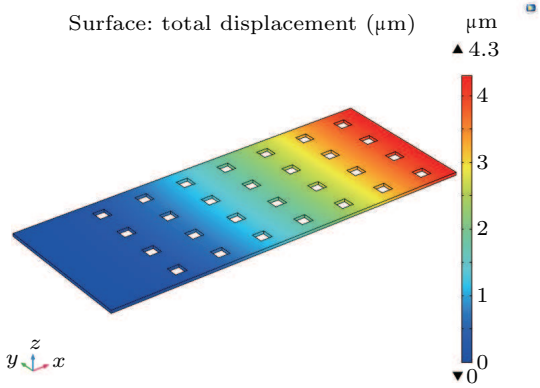


Fig. 3. Displacement simulation of the cantilever beam of the MEMS switch.

The coupling field finite-element software, COMSOL, is used to simulate the cantilever beam of the MEMS switch, and the simulation results are shown in Fig. 3. The cantilever beam deforms under the action of static electricity, and the deformation is largest at its free end. When a distributed load is applied directly under the cantilever beam, the maximum displacement of the cantilever beam in the Z direction is 4.3 μm, which is greater than the distance of 3.0 μm between the switch pull-down electrode and the cantilever beam. We have therefore determined that the structure of the designed switch is reasonable.

2.2. Design of the comb resonator

In this study, a stepped impedance resonator (SIR) is applied to the comb resonator to realize the design of a miniaturized filter. SIRs are divided into the $\lambda_g/4$ type, the $\lambda_g/2$ type, and the λ_g type. The $\lambda_g/4$ type of SIR is selected because of its small size and the location of the center of its second passband at triple the base frequency. The $\lambda_g/4$ type SIR is composed of an open circuit and short circuit in series through an impedance step junction. As shown in Fig. 4, the equivalent impedance and equivalent electrical length of the open-circuit end are (Z_1, θ_1), and the equivalent impedance and equivalent electrical length of the short-circuit end are (Z_2, θ_2), respectively.

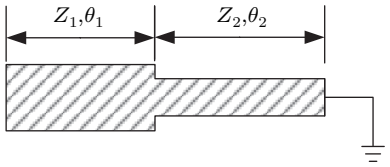


Fig. 4. Schematic of a $\lambda_g/4$-type SIR.

Equation (2) represents the input impedance, ignoring the edge capacitance of the resonator. If the admittance is $Y_i = 1/Z_i = 0$, the $\lambda_g/4$-type SIR resonance condition can be achieved as shown in Eq. (3). Thus, the $\lambda_g/4$-type SIR resonance conditions are related to θ_1, θ_2, and Z_1/Z_2.

$$Z_i = -\mathrm{j} Z_1 \frac{Z_1 \tan\theta_1 + Z_2 \tan\theta_2}{Z_1 - Z_2 \tan\theta_1 \tan\theta_2}, \tag{2}$$

$$\tan\theta_1 \tan\theta_2 = Z_1/Z_2. \tag{3}$$

Equation (4) represents the total electrical length of the $\lambda_g/4$-type SIR. Compared with the electrical length of $\pi/2$ of a uniform impedance resonator (whose open-end width is equal to the short-end width), the SIR normalized resonator length is

$$\theta_{TA} = \theta_1 + \theta_2 = \theta_1 + \tan^{-1}\left(\frac{Z_1}{Z_2 \tan\theta_1}\right). \tag{4}$$

The comb resonator is composed of an arrangement of parallel coupling lines, in which one end is short-circuited and the other end is grounded through the lumped capacitor. Two symmetrical 50 Ω transmission lines are arranged at both ends

of the resonator to form input and output signal ends of the resonator.[22]

In the schematic diagram of the comb resonator in Fig. 5, C_i' represents the load capacitance corresponding to the coupling line in section i, where W_i' represents the width of the coupling line in section i, L_i' represents the length of the coupling line in section i, and $S_{i,i+1}$ represents the interval between the coupling line in section i and section $i+1$ of the resonator. Here, $i = 0$–m. For narrowband comb resonators, the coupling lines from sections one to m are all resonators. The coupling lines of section zero and section $m+1$ feed the external circuit, which changes the impedance instead of acting as a resonator.[23]

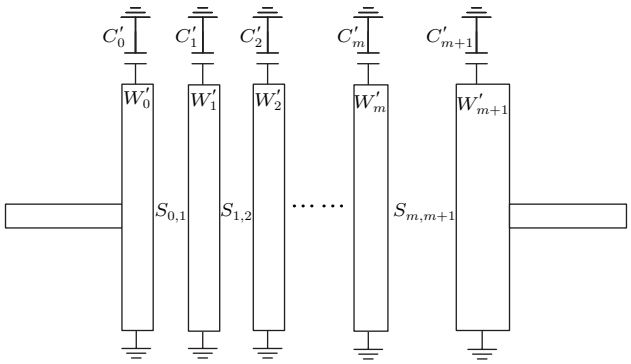


Fig. 5. Schematic diagram of the comb resonator.

Comb resonators have evolved from parallel coupling line resonators, and the central frequency of the resonator is mainly determined by the length of the resonator and the load capacitance. The coupling coefficient and the port load Q value of the resonator can be calculated by[24]

$$K_{i+1} = \frac{BW}{f_0\sqrt{\sigma_i\sigma_{i+1}}} \quad (i = 1, 2, \ldots, m), \tag{5}$$

$$Q_{e1} = \frac{f_0\sigma_0\sigma_1}{BW}, \quad Q_{em} = \frac{f_0\sigma_m\sigma_{m+1}}{BW}, \tag{6}$$

where σ_i is the Chebyshev low-pass prototype value, f_0 is the center frequency of the filter, BW is the passband bandwidth of the filter, and the K level is the coupling coefficient.

2.3. Design of the four-bit filter

Generally, the terminal load capacitance of the comb line is small and fixed. The central frequency of the filter can be adjusted by changing the capacitance if the fixed capacitance is replaced by an adjustable capacitor. Equation (7) shows the relationship between the central frequency of the filter, the resonator length, and the terminal capacitance value:

$$2\pi f_0 \tan(\theta) C = Y_a, \tag{7}$$

where Y_a is the characteristic admittance of the resonator, θ is the electrical length of the resonator, and C is the terminal capacitance.

According to Eq. (7), the inverse relationship between the resonance frequency and the capacitance can be obtained by fixing the electrical length of the resonator and the specific admittance. Based on this characteristic, we designed a reconfigurable bandpass filter. The designed reconfigurable filter consists of eight MEMS switches and comb resonators, and the selection of a specific operating frequency band can be achieved by controlling the gating state of the MEMS switches.

The reconfigurable filter in Fig. 6 is manufactured using MEMS technology and is mainly composed of a substrate and a metal structure.

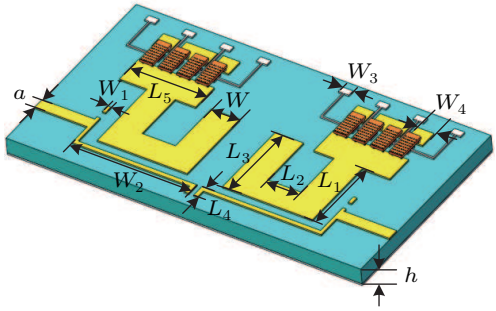


Fig. 6. The structure of the reconfigurable filter.

The filter uses a microstrip line to transmit microwave signals, and the characteristic impedance of its input/output terminals is 50 Ω. By controlling the size of each comb resonator and optimizing the spacing between them, a filter with excellent performance can be obtained. The structural parameters are shown in Table 1.

Table 1. Structural parameters of the reconfigurable comb filter.

Dimension	Value (μm)	Dimension	Value (μm)
L_1	895.5	W	352
L_2	420	W_1	65
L_3	1170	W_2	1506
L_4	168	W_3	200
L_5	592	W_4	226
a	320	h	400

Using the ANSOFT HFSS software, the RF performance of the four-bit filter based on MEMS switches is simulated, and the simulation results are shown in Fig. 7. Figures 7(a)–7(c) show the simulation results for the S_{21}, S_{11} and group delays of the filter, respectively. The filter performance of each switch state is shown in Table 2, where '1' indicates that the switch is on and '0' indicates that the switch is off.

The simulation results indicate that for a frequency range of 7–16 GHz, the maximum insertion loss of the filter is approximately 1.99 dB, the minimum out-of-band rejection is about 18.30 dB, and the maximum bandpass group delay is 0.25 ns. This four-bit filter exhibits excellent performance among reconfigurable bandpass filters, and the proposed filter can switch 16 channel frequencies with fewer switches.

Table 2. Corresponding filter performance of each switch state. $f_{1/2}$ is the frequency point of the sideband.

State	f_0 (GHz)	Insertion loss (I.L.) (dB)	Rejection out-of-band @($f_{1/2} \pm 0.5$ GHz) (dB)	Bandpass group delay (ns)
0000	8.16	1.99	≥ 28.90	≤ 0.25
0001	14.14	1.53	≥ 19.78	≤ 0.12
0010	14.51	1.51	≥ 18.41	≤ 0.14
0011	14.64	1.28	≥ 19.16	≤ 0.15
0100	14.52	1.42	≥ 18.30	≤ 0.14
0101	14.85	1.16	≥ 19.35	≤ 0.17
0110	14.79	1.23	≥ 19.14	≤ 0.16
0111	14.87	1.14	≥ 19.55	≤ 0.18
1000	14.31	1.45	≥ 18.62	≤ 0.14
1001	14.94	1.12	≥ 19.46	≤ 0.19
1010	14.84	1.08	≥ 20.41	≤ 0.18
1011	14.97	1.10	≥ 20.47	≤ 0.20
1100	14.59	1.02	≥ 19.53	≤ 0.17
1101	14.99	1.08	≥ 19.90	≤ 0.18
1110	14.91	1.10	≥ 19.32	≤ 0.18
1111	15.00	1.06	≥ 20.04	≤ 0.19

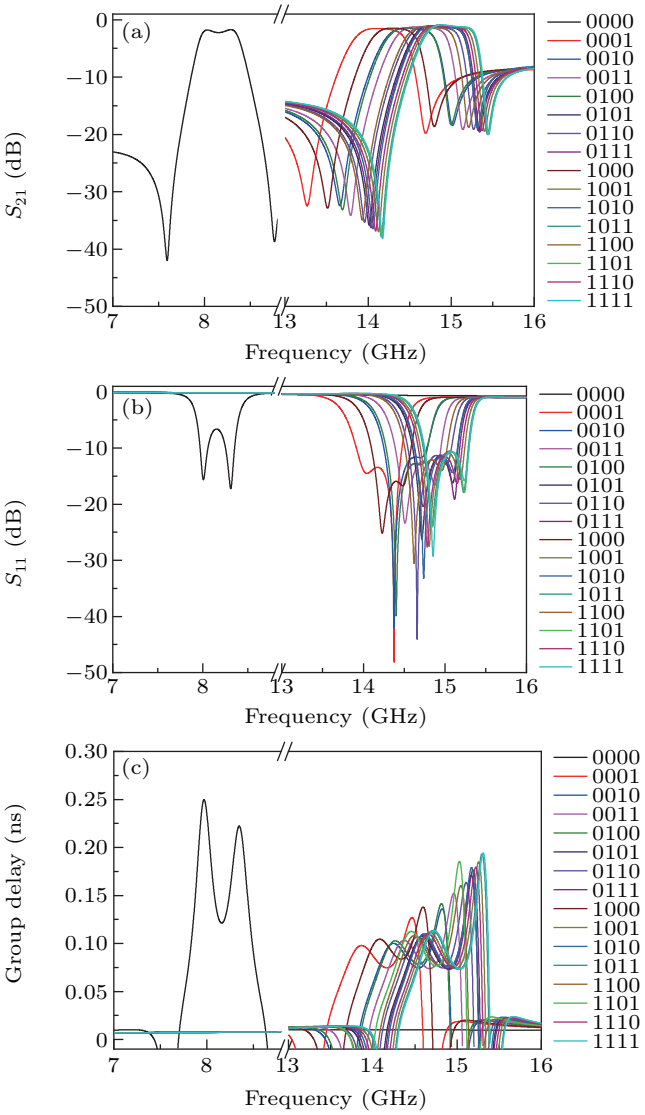


Fig. 7. Simulation results for the filter: (a) S_{21}, (b) S_{11}, and (c) group delay.

Table 3 provides a comparison between the results for currently used reconfigurable filters and the filter designed in this study. As can be seen from Table 3, the proposed filter is able to switch 16 channel frequencies with the least number of switches, thus improving the reliability of the filter. Compared with current reconfigurable band-pass filters, the proposed filter has the advantages of low insertion loss, small size, and high integration.

Table 3. Comparison of reconfigurable bandpass filters.

Ref.	f_0 (GHz)	I.L. (dB)	Channel No.	Switch No.	Size (mm^2)
2005[19]	6.54–9.73	3–4	16	20	5×4
2008[25]	4.17–5.91	1.53–2.75	8	10	$\sim 10 \times 9$
2015[14]	0.90–2.35	1.4–4.9	2	3	97×32
2016[26]	21.69–24.36	2.81–4.03	4	2	1.56×1.46
2017[15]	$\sim$ 7.81–8.35	~ 3	2	4	25×17
This work	8.16–15.00	1.02–1.99	16	8	4.4×2.5

2.4. Fabrication and measurement of the RF MEMS switch

The MEMS switch, as the core device of the reconfigurable filter, is fabricated using micro–nano surface technology. Figure 8 illustrates the fabrication process of the MEMS switch.

First, a thermal oxide layer is grown by a wet etching process on a silicon wafer with a thickness of 400 μm. Second, a silicon nitride layer is deposited by plasmaenhanced chemical vapor deposition (PECVD). Third, a square silicon nitride layer is etched by reactive ion etching (RIE). Fourth, an aluminum (Al) layer is sputtered by magnetron sputtering to fabricate the drive electrode. Subsequently, an Au layer with a thickness of 2 μm is plated to fabricate the transmission line of the MEMS switch. Then, a polyimide (PI) sacrificial layer is spun and cured. Next, on the sacrificial layer, an Au layer with a thickness of 2 μm is electroplated to fabricate the top electrode. Finally, the sacrificial layer is released by RIE, and the MEMS switch is finally fabricated.

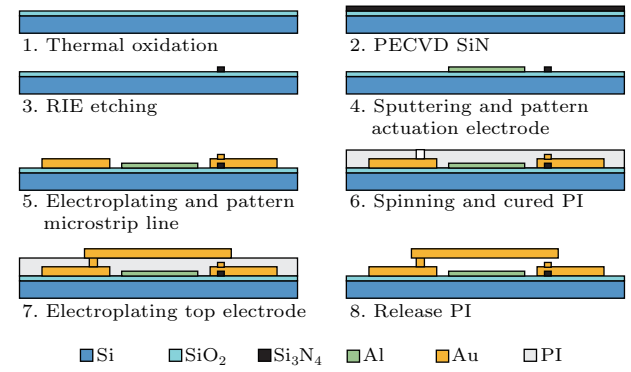


Fig. 8. The fabrication processes of the MEMS switch.

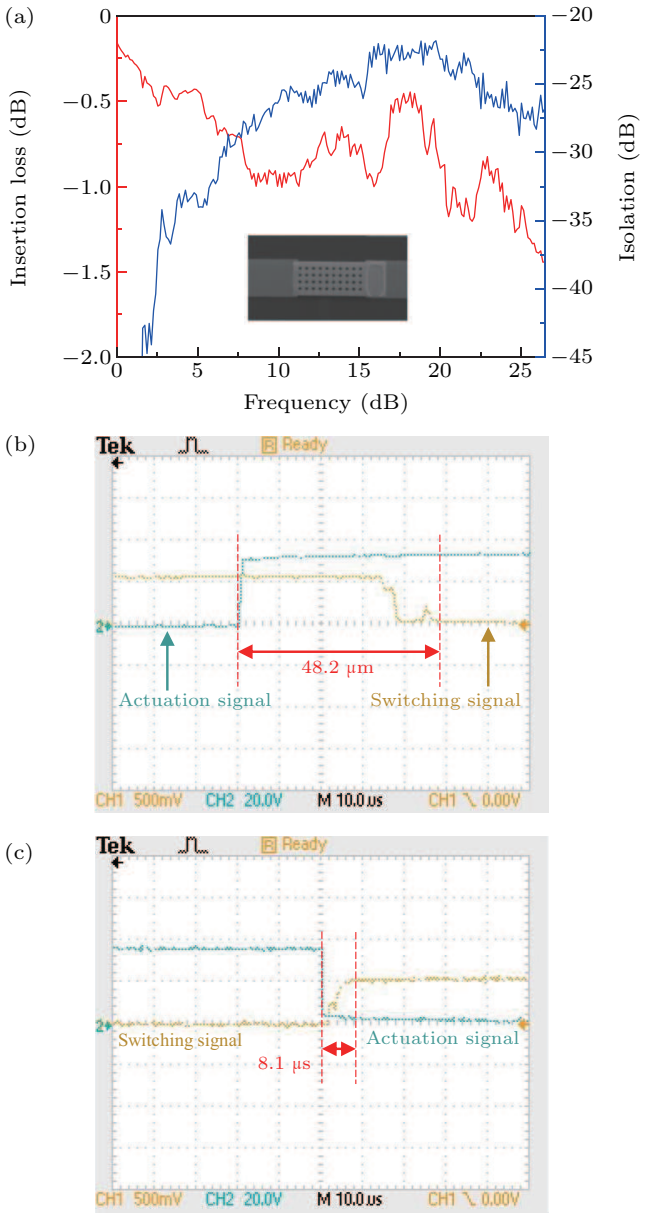


Fig. 9. Measured results of the MEMS switch: (a) S_{21}, (b) switching on time and (c) switching off time.

The measured results in Fig. 9(a) show that the insertion loss of the MEMS switch is approximately 1.0 dB and the isolation is more than 22.0 dB in the range of 7–16 GHz, which satisfy the design specification requirements. Figures 9(b) and 9(c) show the switching on and switching off times of the switch, respectively. As the actuation signal rises from zero to the signal voltage, the switch starts to pull down and achieves a stable contact after multiple bounces; and the switching on time of the switch is about 48.2 μs. When the actuation signal drops from the pull-down voltage to zero, the switching off of the switch from the "on" state to the "off" state takes about 8.1 μs. On the other hand, reliability is a key metric of a MEMS reconfigurable filter, and the switching life of a MEMS switch can be up to 10^7 times. After many tests, the insertion loss changed little and the repeatability was good, which confirms the performance of the reconfigurable filter.

3. Conclusions and perspectives

In this study, the current development status of reconfigurable filters is first analyzed, and then a four-bit bandpass filter with a small size, low loss, and strong reconfigurability is designed. The terminal load capacitance of the comb resonator can be changed by MEMS switches, thus tuning the filter. The results show that this filter has good performance within a 7–16 GHz operational frequency range and can be used in multi-frequency complex communication systems. As a result, it has great potential for use in channel selection, image suppression, duplexing, and multichannel communication.

Acknowledgments

Project supported by the National Defense Technology Industry Strong Foundation Project of China (Grant No. JCKY2018∗∗∗∗06) and the Information System New items Project (Grant Nos. 2018∗∗∗∗26 and 2019∗∗∗∗10). We thank the Key Laboratory of Instrumentation Science and Dynamic Measurement for their support.

References

[1] Tao L, Wei B, Guo X B, Li H C, Luo C J and Chao B S 2020 *Chin. Phys. B* **29** 068502
[2] Chang E W and Lin Y S 2018 *IEEE Access* **6** 73637
[3] Wu D, Wei B, Li B, Guo X B, Lu X X and Cao B S 2018 *Chin. Phys. B* **27** 068502
[4] Wu D, Wei B, Lu X L, Lu X X, Guo X B and Cao B S 2018 *Chin. Phys. B* **27** 068503
[5] Song K and Xue Q 2010 *IEEE Trans. Microwave Theory Tech.* **58** 978
[6] Bukuru D, Song K, Zhang F, Zhu Y and Fan M 2017 *IEEE Trans. Microwave Theory Tech.* **65** 783
[7] Gao T, Wei B and Heng Y 2017 *Chin. Phys. B* **26** 058503
[8] Mo Y, Song K and Fan Y 2014 *IEEE Microw. Wirel. Compon. Lett.* **24** 333
[9] S Wang X, Wei B, Lu X L, Guo X B and Cao B S 2017 *Chin. Phys. B* **26** 128501
[10] Gao T Q, Wei B and Heng Y 2017 *Chin. Phys. B* **26** 058503
[11] Ebrahimi A, Withayachumnankul W, Al-Sarawi S F and Abbott D 2016 *IEEE Microw. Wirel. Compon. Lett.* **26** 571
[12] Hinojosa J, Rossi M, Saura-Ródenas A, Álvarez-Melcón A and Martínez-Viviente F L 2018 *IEEE Trans. Microwave Theory Tech.* **66** 3001

[13] Deng L, Li D Z, Liu Z L, Meng Y H, Guo X N and Tian Y H 2017 *Chin. Phys. B* **26** 024209

[14] Chuang M L and Wu M T 2015 *IEEE Trans. Circuits Syst. II-Express Briefs* **62** 347

[15] Zhang N B, Mei L R, Wang C T, Deng Z L, Yang J and Guo Q Q 2017 *IEEE Transactions on Electron Devices* **64** 3377

[16] Shojaei-Asanjan D and Mansour R R 2017 *IEEE Microw. Mag.* **18** 100

[17] Kumar N and Kumar Y 2017 *IEEE Trans. Microwave Theory Tech.* **65** 3824

[18] Hu F R, Xu X, Li P, Xu X L and Wang Y E 2017 *Chin. Phys. B* **26** 074219

[19] Entesari K and Rebeiz G M 2005 *IEEE Trans. Microwave Theory Tech.* **53** 1103

[20] Li M W, Liu Q H, Wu Q N and Han Y P 2018 *Microsyst. Technol.* **25** 1619

[21] Li M W, Zhang Y F, Zhao Y L, Xue P F and Wu Q N 2020 *Analog Integr. Circuits Process.* **102** 617

[22] Zai Q H 2016 *Design and Realization on Silicon-based MEMS Microwave Bandpass Filter* (MS disscrtation) (Taiyuan: North University of China) (in Chinese)

[23] Chaubey M K and Bhadauria A 2018 *IOP Conf. Ser.: Mater. Sci. Eng.* **331** 012030

[24] Hong J S 2001 *Microstrip Filters for RF/ Microwave Applications* (Vol. 1) (New York: Wiley) pp. 235–271

[25] Park S J, El-Tanani M A, Reines I and Rebeiz G M 2008 *IEEE Trans. Microwave Theory Tech.* **56** 2348

[26] Deng Z L, Wei H and Guo X B 2016 *Micromachines* **7** 149